0026-895X/97/050872-10$3.00/0

MOLECULAR PHARMACOLOGY, **51**:872–881 (1997).

Inhibition of Recombinant Ca^{2+} Channels by Benzothiazepines and Phenylalkylamines: Class-Specific Pharmacology and Underlying Molecular Determinants

DONGMING CAI, JENNIFER G. MULLE, and DAVID T. YUE

Program in Molecular and Cellular System Physiology, Department of Biomedical Engineering, The Johns Hopkins University School of Medicine, Baltimore, Maryland 21205

Received December 11, 1996; Accepted February 13, 1997

SUMMARY

To understand the molecular basis of state-dependent pharmacological blockade of voltage-gated Ca^{2+} channels, we systematically characterized phenylalkylamine and benzothiazepine inhibition of three molecular classes of Ca^{2+} channels (α_{1C}, α_{1A}, and α_{1E}) expressed from cDNA clones transfected into HEK 293 cells. State-dependent blockade figures importantly in the therapeutically desirable property of use-dependent drug action. Verapamil (a phenylalkylamine) and diltiazem (a benzothiazepine) were imperfectly selective, so differences in the state dependence of inhibition could be compared among the various channels. We found only quantitative differences in pharmacological profile of verapamil: half-maximal inhibitory concentrations spanned a 2-fold range (70 μM for α_{1A}, 100 μM for α_{1E}, and 110 μM for α_{1C}), and inhibition was state dependent in all channels. In contrast, diltiazem produced only state-dependent block of α_{1C} channels; α_{1A} and α_{1E} channels demonstrated state-independent block despite similar half-maximal inhibitory concentrations (60 μM for α_{1C}, 220 μM for α_{1E}, and 270 μM for α_{1A}). To explore the molecular basis for the sharp distinction in state-dependent inhibition by diltiazem, we constructed chimeric channels from α_{1C} and α_{1A} and localized the structural determinants for state dependence to repeats III and IV of α_{1C}, which have been found to contain the structures required for benzothiazepine binding. We then constructed a mutant α_{1C} construct by changing three amino acids in IVS6 (Y1490I, A1494S, I1497M) that have been implicated as key coordinating sites for avid benzothiazepine binding. Although these mutations increased the half-maximal inhibitory concentration of diltiazem inhibition by ~10-fold, the state-dependent nature of inhibition was spared. This result points to the existence of physically distinct elements controlling drug binding and access to the binding site, thereby favoring a "guarded-receptor" rather than a "modulated-receptor" mechanism of drug inhibition.

Pharmaceutical agents that modulate voltage-gated Ca^{2+} channels have found widespread application as basic research tools and therapeutic drugs. From the biophysical perspective, L-type Ca^{2+} channel modulation by the most established generation of organic Ca^{2+} channel blockers (dihydropyridines, phenylalkylamines, and benzothiazepines) provides rich experimental models of allosteric modification of gating and/or physical blockade of the conduction pathway. In physiological experiments, these organic compounds, together with neuroactive peptides that block specific molecular classes of Ca^{2+} channels (1), have been used to delineate the contributions of different channel types to specific biological functions. In the clinical setting, members of each of the three classes of organic compounds act on L-type channels to treat disorders as varied as angina, hypertension, and cardiac arrhythmia (2–4). Moreover, recombinant neuropeptides that inhibit neuronal N-type channels hold promise for the treatment of chronic intractable pain (5). Finally, mutations in neuronal P/Q-type channels have been linked to a inherited forms of migraine and ataxia (6), raising the possibility that as-yet-undiscovered compounds that select for P/Q channels may provide novel therapies for the more general forms of these neurological disorders. For all these reasons, there is enormous interest in understanding the molecular basis of Ca^{2+} channel inhibition and discovering new compounds with high specificity for selected molecular classes of Ca^{2+} channels.

The cloning and expression of several classes of Ca^{2+} channels provide powerful tools for addressing just these issues. First, mutant and chimeric Ca^{2+} channel analysis on the main $\alpha 1$ subunits have already revealed several key amino acid residues that can account for much of the class-specific difference in binding affinity of dihydropyridines (7–9), phe-

This work was supported by Specialized Center of Research in Sudden Cardiac Death Grant NIH P50-HL52307 (D.T.Y.) and Postdoctoral Training Fellowship NIH 5-T32-HL07581 (D.M.C.).

ABBREVIATIONS: HEK, human embryonic kidney; PCR, polymerase chain reaction; EGTA, ethylene glycol bis(β-aminoethyl ether)-*N*,*N*,*N*′,*N*′-tetraacetic acid; HEPES, 4-(2-hydroxyethyl)-1-piperazineethanesulfonic acid.

nylalkylamines (9–11), and benzothiazepines (12, 13). Second, the ability to express a homogeneous population of a selected type of channel, in the virtual absence of contaminating currents, provides an ideal opportunity to assess the relative effect of an agent on a particular class of Ca^{2+} channel. The coexistence of multiple channel types in neurons and other native cells may complicate quantitative attribution of drug inhibition to particular channel types.

Despite the rapid advances and molecular approaches outlined above, there is still little understanding of the molecular mechanism of Ca^{2+} channel inhibition. All recombinant channel studies to date have focused mainly on simple differences in the potency of inhibition of different recombinant Ca^{2+} channels by various organic blockers. No systematic comparison has been made of the characteristic phenotype of block. In particular, there is little information on the relative state dependence of block, a feature that is critical to the therapeutically useful property of "use dependence" (16, 17). Use-dependent blockers preferentially inhibit channels during unusually high electrical activity, as found in a cardiac arrhythmia or seizure focus. Differences in state-dependent block among the various recombinant channels could point the way to the structural determinants of use dependence. These molecular elements may be distinct from the structures that specify simple binding affinity according to the guarded-receptor hypothesis (18).

Here, we report the systematic characterization of phenylalkylamine and benzothiazepine inhibition of three molecular classes of Ca^{2+} channels expressed in HEK 293 cells from cDNA clones encoding α_{1A}, α_{1E}, and α_{1C} subunits. The first two $\alpha 1$ clones correspond to neuronal P/Q-type and R-type channels (19), and the latter clone corresponds to cardiac L-type channels. We chose to study these two classes of organic compounds because they proved to be imperfectly selective, so differences in the state dependence of block could be compared among the various classes of Ca^{2+} channels. Dihydropyridines were almost perfectly selective for L-type channels (7; but see 14, 15), so no such comparison can be made.

Materials and Methods

Expression of recombinant voltage-gated Ca^{2+} channels. cDNAs encoding calcium channel α_1, β_{2a} (20), and α_2 (21) subunits were subcloned into mammalian expression plasmids. α_{1C} (22), α_{1E} (23), and β_{2a} were subcloned into cytomegalovirus-promotor expression plasmid pGW1H (British Biotechnologies, Oxford, UK); α_{1A} (24, 25), as well as chimeric and/or mutant α_1 subunits (α_{1CCAA}, α_{1AACC}, and $\alpha_{1C\text{-}ISM}$, as described below), was subcloned into CMV-promotor expression plasmid pcDNA3 (InVitrogen Corporation, San Diego); and α_2 was subcloned in the constitutively active, metallothionein-promotor expression plasmid pZEM229R (Zymogenetics, Seattle, WA). Low-passage-number (< 20) HEK 293 cells, obtained from Dr. Jeremy Nathans (26), were transiently transfected with plasmids containing α_1 and β_{2a} subunits (10 μg each/10-cm plate) using a calcium-phosphate precipitation procedure (27). With chimeric channels, the α_2 subunit and pAdVAntage vector (Promega, Madison, WI) were sometimes cotransfected (10 and 5 μg/10-cm plate, respectively) to enhance expression, as noted. Cotransfection of the α_2 subunit had no detectable effect on the pharmacological profile of diltiazem (not shown). pAdVAntage encodes the transcription-enhancing genes *VAI* and *VAII* from the adenovirus genome (28). Recombinant currents were observed in > 30% of transfected cells for the majority of constructs; transfection with a β-galactosidase reporter gene resulted in a > 50% overall expression rate.

Mock-transfected cells were cotransfected with β_{2a} and α_2 subunits. No high-voltage-activated channels were detected (n = 25 cells in three rounds of transfection). In mock-transfected cells, we occasionally (~10–20% of cells) observed endogenous, low-voltage-activated Ca^{2+} currents of small amplitude. Although endogenous currents of such small amplitude would contribute negligibly to most of our results, such cells were nevertheless rejected. Therefore, all data reflect the expression of recombinant Ca^{2+} channels.

Construction of mutant and chimeric Ca^{2+} channel α_1 subunits. Chimeric Ca^{2+} channels were generated in which repeats I and II were interchanged between α_{1C} and α_{1A}, yielding α_{1CCAA} and α_{1AACC} (see Fig. 8, *top*). To construct α_{1CCAA}, we amplified a region spanning repeats III and IV of α_{1A} (nucleotides 2024–6639, with nucleotide 1 at the start codon, here and throughout), using PCR catalyzed by *Pfu* DNA polymerase (Stratagene, La Jolla, CA). The PCR product was initially blunt-end-ligated into pCR-Script using a commercial cloning kit (Stratagene). PCR primers contained flanking *Eco*RI and *Xba*I restriction endonuclease sites, enabling transfer of the PCR product into unique sites on the α_{1C} construct. The resulting chimeric channel contained amino acids 1–746 from α_{1C}, followed by 675-2213 from α_{1A}. To construct α_{1AACC}, we PCR-amplified a region spanning repeats III and IV of α_{1C} (nucleotides 3198–5193). PCR primers contained flanking *Acc*I and *Xba*I restriction sites, permitting ready transfer of the PCR product into these sites on the α_{1A} construct. The resulting construct contained amino acids 1–1335 of α_{1A}, followed by 1067–1732 of α_{1C} and a premature stop codon. The premature stop codon was designed so as to delete the last 439 amino acids of the α_{1C} carboxyl tail because it has been previously demonstrated that such truncation significantly enhances expression of current without an appreciable change in pharmacological profile (29).

We generated a mutant α_{1C} construct in which three amino acids in the IVS6 region were changed (Y1490I, A1494S, I1497M, numbering relative to α_{1C}) to those found in analogous positions of α_{1A}, yielding the mutant construct $\alpha_{1C\text{-}ISM}$. To facilitate mutagenesis, two silent mutation were introduced into the standard α_{1C} construct (C4974T and G4977A), yielding a unique *Sfu*I restriction site at nucleotide 4973. In the resulting $\alpha_{1CSfuI+}$ construct, the IVS6 region was now bracketed by unique *Eco*RV and *Sfu*I restriction sites, which are separated by only 626 base pairs. To generate $\alpha_{1C\text{-}ISM}$, we used PCR mutagenesis by overlap extension (30). The outside primers contained *Eco*RV and *Sfu*I restriction sites, permitting transfer of the PCR product (containing the desired mutations) into these sites on $\alpha_{1CSfuI+}$. Portions of chimeric and mutant channel constructs derived from PCR were verified in their entirety with the use of the fluorescent dideoxy terminator method of thermocycle sequencing on an automated DNA sequencer (Applied Biosystems Division 373a; Perkin-Elmer Cetus, Norwalk, CT)

Electrophysiology. Whole-cell recordings were conducted at room temperature 1–3 days after transfection. The external solution contained 150 mM *N*-methyl-D-glucamine aspartate, 10 mM glucose, 10 mM HEPES, 10 mM 4-aminopyridine, and 0.1 mM EGTA, pH 7.3–7.4 with 1 M *N*-methyl-D-glucamine aspartate; 2–30 mM $CaCl_2$ or $BaCl_2$ was added as charge carrier. The internal solution contained 135 mM Cs-methanesulfonate, 5 mM CsCl, 10 mM EGTA, 10 mM HEPES, 1 mM $MgCl_2$, and 4 mM MgATP, pH 7.2–7.3 with CsOH.

L-type Ca^{2+} channel antagonists, verapamil (Calbiochem, La Jolla, CA), and diltiazem (Sigma Chemical, St. Louis, MO), were dissolved in distilled water to make stock solutions (10 mM or 1 M) that were stored at −20°. Aliquots were diluted to the external solution to obtain the final desired concentrations.

For convenience, both Ca^{2+} and Ba^{2+} were used as charge carriers. Although an earlier study reported that the potency of Ca^{2+} channel blockers was modulated by the extracellular concentration and species of charge carrier (31), we found no evidence for such modulatory effects on α_{1C} and α_{1A} channels with the use of verapamil

and diltiazem. We found that neither concentration (Ca^{2+}, 5 versus 30 mM) nor charge species (5 mM Ca^{2+} versus 5 mM Ba^{2+}, or 30 mM Ca^{2+} versus 30 mM Ba^{2+}) significantly altered the extent of blockade by verapamil or diltiazem. Similar results were reported in the study of dihydropyridines (32, 33).

Transfected HEK 293 cells were grown onto coverslips, which facilitated easy transfer to a recording chamber just before electrophysiological recording. Fresh external solution continuously perfused the chamber at a flow rate of 1–2 ml/min. The bath was grounded by a 0.5 M KCl agar bridge attached to a Ag-AgCl wire. Whole-cell current records were obtained by standard patch-clamp techniques. Series resistance was typically < 5 MΩ and compensated $> 60\%$. Leak and capacity transients were assessed between each test depolarization by a P/8 protocol and subtracted from test currents in all subsequent data analysis. Currents were filtered at 2 kHz (−3 dB, four-pole Bessel), sampled at 10 kHz, and stored digitally for data analysis.

Statistical analysis. All pooled data are reported as mean ± standard error. Statistical significance was assessed by two-sided, paired *t* test, with $p < 0.05$ taken as the minimal level of significance. N.S. denotes a comparison with no statistical significance ($p > 0.05$).

Results

Verapamil and diltiazem inhibition of multiple classes of Ca^{2+} channels. Although verapamil was developed as a blocker of L-type Ca^{2+} channels, Fig. 1 illustrates that the identical concentration of this compound (50 μM) produced significant block of all three classes of channels tested. The pharmacological profiles of α_{1C}, α_{1A}, and α_{1E} are presented in three columns, as labeled. The exemplar currents at the top, taken before and during application of verapamil (Fig. 1, A–C), explicitly demonstrate the inhibition of each type of channel. The diary plots of peak current shown below indicate the rapid inhibition of current on exposure to verapamil (●), which is readily reversed on wash with control solution (△), except in the case of α_{1C}. Slow or incomplete reversal of block was characteristic of α_{1C}.

Apart from inhibition of peak current, a notable effect of verapamil was to accelerate the decay of current during maintained step depolarization. This effect is apparent in the exemplar traces (*top*, A–C), as well as in the diary plots of the fraction of peak current remaining at the end of 100-msec depolarizing steps (Fig. 1, D–F, r_{100}). This acceleration of the decay of current is consistent with a state-dependent blocking mechanism in which verapamil preferentially inhibits the channel when it resides in or near the open and/or inactivated state. Such preferential inhibition of open/inactivated states could underlie the substantial use-dependent component of block observed in all channels with our 1/15 Hz stimulation frequency (data not shown). Overall, there was no fundamental difference in the action of verapamil on the three classes of channels.

In contrast, diltiazem produced fundamentally different effects on α_{1C} compared with α_{1E} or α_{1A} channels. Fig. 2 summarizes the pharmacological profile of diltiazem, following the same format as in Fig. 1. Although peak currents were readily inhibited by 100 μM diltiazem for all three channels (Fig. 2, A–C), the acceleration of current decay during maintained depolarizing steps was present in only α_{1C}. The latter finding is demonstrated by the exemplar records (*top*, A–C), as well as in the diary plots of r_{100} (D–F). The flat r_{100} plots for α_{1A} (Fig. 2E) and α_{1E} (Fig. 2F) quantitatively demonstrate the lack of change in current waveform with diltiazem exposure. These results suggested that diltiazem might selectively demonstrate preferential open/inactivated-state block of α_{1C} but not α_{1A} and α_{1E} channels. This idea was consistent with the absence of appreciable use-dependent block with α_{1A} and α_{1E} channels (data not shown). If confirmed, such a clearcut distinction in fundamental action could permit structural analysis of the basis of state-dependent block by diltiazem.

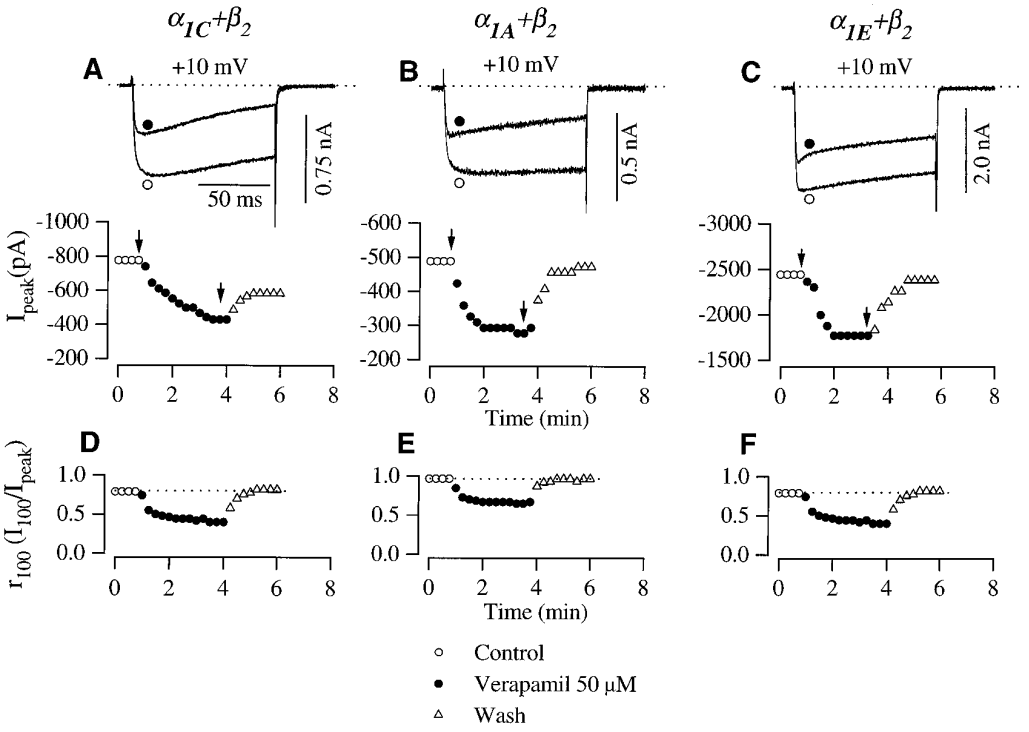

Fig. 1. Verapamil inhibition of multiple classes of Ca^{2+} channels. *Top* (A–C), exemplar current traces from (A) α_{1C}, (B) α_{1A}, and (C) α_{1E}, all coexpressed with β_2, in the (○) absence and (●) presence of 50 μM verapamil. The charge carrier was 5 mM Ca^{2+}, and currents were evoked every 15 sec by 100-msec depolarizing pulses from a holding potential of −80 mV. *Bottom* (A–C), diary plots of peak current (○) before, (●) during, and (△) after exposure to 50 μM verapamil. *Arrows*, traces shown above. D–F, Diary plots of r_{100}, the fraction of peak current remaining at the end of 100-msec depolarization. Plots quantify the enhancement of current decay during verapamil inhibition. Results for α_{1C}, α_{1A}, and α_{1E} are representative of those observed in a total of seven, four, and five cells, respectively.

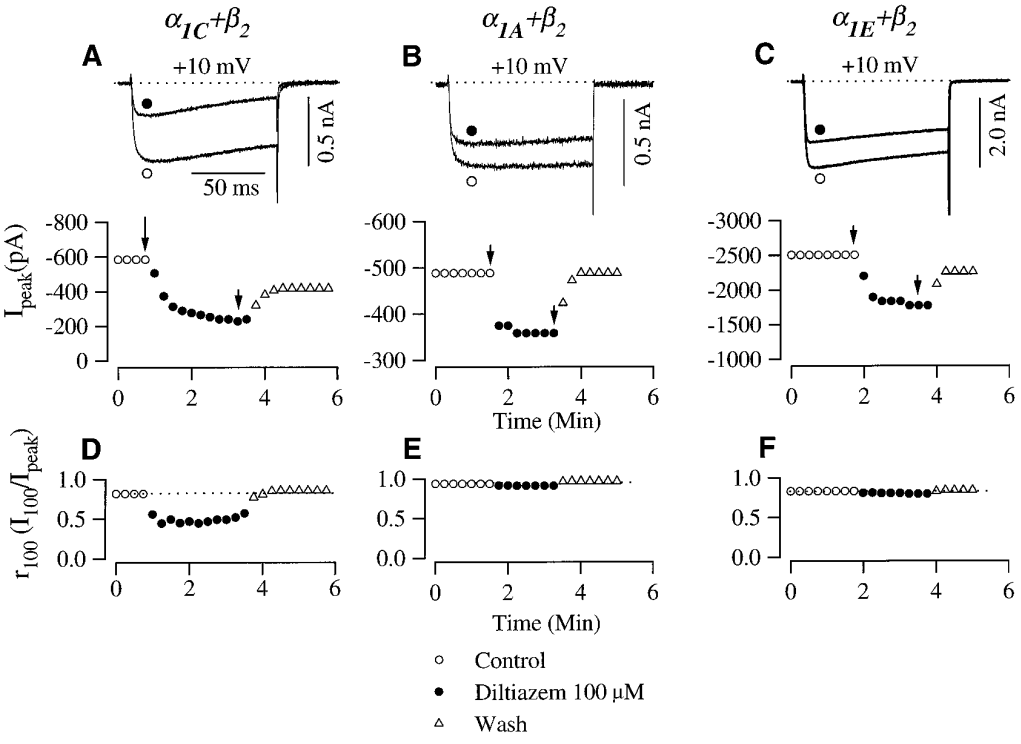

Fig. 2. Diltiazem inhibition of multiple classes of Ca^{2+} channels. The format is identical to that in Fig. 1, except that channels were inhibited by 100 μM diltiazem. Results for (A) α_{1C}, (B) α_{1A}, and (C) α_{1E} are representative of those observed in a total of four, four, and seven cells, respectively.

Dose-response curves for verapamil and diltiazem block. As another potential test for state-dependent block in a given drug/channel combination, we characterized the dose dependence of blockade by verapamil and diltiazem for all three types of channels. If a drug binds with different affinity to channels in distinct conformations, then the dose-response curve for drug blockade might be described by multiple binding isotherms corresponding to various channel states. On the other hand, if a drug binds with the same affinity, regardless of channel state, then the dose-response relation should describe a single Langmuir function.

Fig. 3 shows the dose-response of verapamil and diltiazem blockade for the three types of Ca^{2+} channels. In each case of verapamil blockade, fits of relations with single binding isotherms (not shown) consistently underestimated the degree of block in the 1–10 μM range, with differences between data and theoretical predictions ("residuals") ranging between 0.1 and 0.2. In contrast, fits with functions composed of two binding isotherms (*solid gray curves*) yielded no such consistent deviations in residuals, as if channels were roughly distributed among two groups of states: one with a high affinity for verapamil and the other with low affinity. These results fit nicely with the consistent acceleration of current decay produced by verapamil on all three classes of channels (Fig. 1). Therefore, both dose-response (Fig. 3A) and r_{100} data (Fig. 1, D–F) were consistent with state-dependent blockade of all three channels by verapamil.

The form of dose-response relations for diltiazem inhibition also agreed with our initial assignment of state-dependent block to α_{1C} (Fig. 2D), and state-independent block to α_{1A} (Fig. 2E) and α_{1E} (Fig. 2F). The α_{1C} data were well fit by a relation with two binding isotherms (Fig. 3B, *top*), which is consistent with the channel being distributed between higher and lower affinity states. Fits of relations with one binding isotherm (not shown) yielded consistent deviations in residuals, as observed above with verapamil. In contrast, the α_{1A} and α_{1E} dose-response data were well fit by a single binding term (Fig. 3B, *middle* and *bottom*), as if diltiazem had an equal affinity for all states.

Holding-potential dependence of drug inhibition. Another critical test for state-dependent block in certain drug/channel combinations is to determine whether the degree of drug inhibition is dependent on the holding potential between voltage pulses (32, 34). So far, all of our experiments were conducted with a fixed holding potential of −80 mV. At different holding potentials, the distribution of channels among various states was likely to be different. Consequently, if a drug bound with different affinity to different states, then the degree of inhibition would be affected by holding potential. Alternatively, if the drug bound with equal affinity to all states, no such holding potential dependence would be observed.

Fig. 4 shows the effects of holding potential on verapamil inhibition. The schematic (*top*) represents the holding potentials used in the various phases of the protocol. Brief test pulses were delivered every 15 sec from the indicated holding potentials. Because all measurements were taken over a short time period, we minimized the effects of drift and rundown. Before the application of verapamil, the holding potential was initially set at a depolarized level (−60 mV for α_{1C} and α_{1A}; −80 mV for α_{1E}), where the channel populated deep resting, shallow resting, and inactivated states. After stabilization at this potential (○), we set the holding potential to a hyperpolarized value (−100 mV for α_{1C} and α_{1A}; −110 mV for α_{1E}) while still in the absence of verapamil. After equilibration (△), inactivation was minimal, and most channels were in a deep resting state. The control currents obtained at these two potentials served to normalize currents inhibited by verapamil. While maintaining the hyperpolarized holding potential, verapamil was then applied, and the

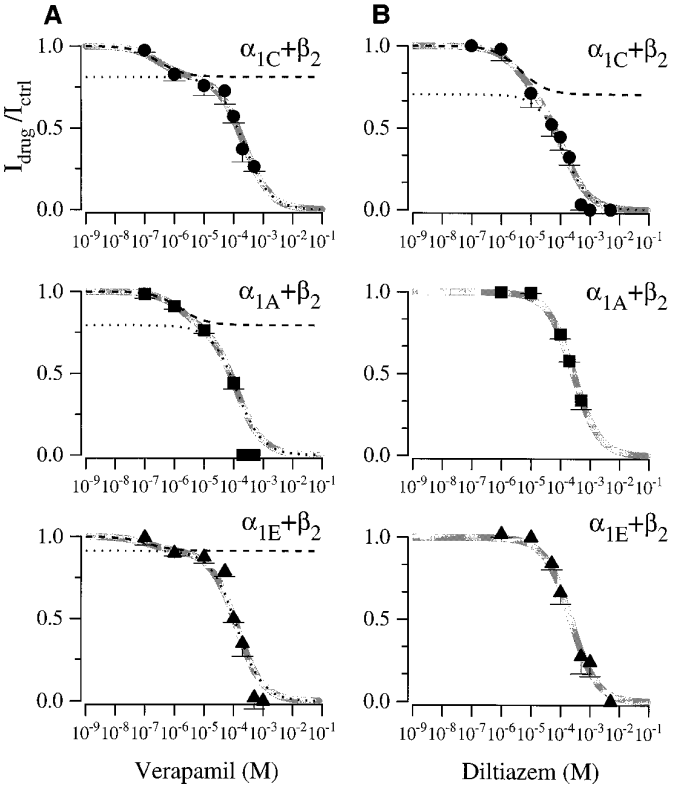

Fig. 3. Concentration dependence of verapamil and diltiazem inhibition. *Ordinate*, peak current during steady state exposure to the blockers, normalized by the peak current before drug exposure, defined as I_{drug}/I_{ctrl}. *Points,* mean ± standard error obtained from three to five cells. We applied only one concentration of drug to each cell, and the extent of drug block was measured as soon as peak currents showed no visible change from one pulse to the next. We thereby minimized possible distortion that might have occurred with a cumulative dose-response protocol, in which variable rundown could complicate interpretation. A, In each case of verapamil blockade, data were fit by a dual binding-site relation: $I_{drug}/I_{ctrl} = 1 - f_1*[drug]/([drug] + K_{d1}) - f_2*[drug]/([drug] + K_{d2})$, where $f_1 + f_2 = 1$, and f_1 and f_2 represent the fraction of channels in high and low affinity binding conformations, respectively; and K_{d1} and K_{d2} represent dissociation constants for high and low affinity states, respectively. Dose-response relations for channels with high and low affinity states would be described by this two-isotherm relation as long as equilibration of drug binding is rapid relative to exchange between high and low affinity states. *Solid gray curve*, fit of this relation. *Dashed and dotted curves*, contribution of individual binding isotherms. A computer-based, iterative, nonlinear fitting algorithm was used. For α_{1C}, $K_{d1} = 0.29$ μM, $K_{d2} = 220$ μM, $f_1 = 0.19$, and $f_2 = 0.81$. For α_{1A}, $K_{d1} = 1.57$ μM, $K_{d2} = 124$ μM, $f_1 = 0.21$, and $f_2 = 0.79$. For α_{1E}, $K_{d1} = 0.13$ μM, $K_{d2} = 123$ μM, $f_1 = 0.09$, and $f_2 = 0.91$. When fits were performed with a one binding isotherm, there was a consistent deviation in residuals (theoretical prediction-data ~0.1 to 0.2) in the 1–10 μM range for all three channels. We observed no such consistent deviation in residuals with fits of the two-binding-isotherm function. For all data, currents were elicited by depolarizations to +10 mV, delivered every 15 sec from a holding potential of −80 mV, with 2 mM Ca^{2+} as charge carrier. B, Concentration dependence of diltiazem inhibition. The format is identical to that in A, except that single-binding isotherms were used to fit the data for α_{1A} and α_{1E} ($I_{drug}/I_{ctrl} = K_{d1}/([drug] + K_{d1})$). The fit parameters were as follows. For α_{1C}, $K_{d1} = 4.48$ μM, $K_{d2} = 129$ μM, $f_1 = 0.29$, and $f_2 = 0.71$. For α_{1A}, $K_{d1} = 270$ μM. For α_{1E}, $K_{d1} = 220$ μM. In the case of α_{1C}, the fit with a single-binding isotherm function consistently showed a residual theoretical prediction-data) averaging −0.15 at 10 μM diltiazem. No such deviation in residuals was observed with two-binding-isotherm fit shown (*top*, *solid gray curve*). For α_{1A} and α_{1E}, fits of a single binding isotherm (*solid gray curves*, *middle* and *bottom*, respectively) showed no consistent deviation of residuals.

steady state level of inhibition was allowed to develop (▲). The holding potential was then adjusted to the initial depolarized level and the steady level of inhibition allowed to develop with verapamil still present (●). Verapamil was then removed, and the current allowed to recover at the depolarized (*cross-centered circle*) and hyperpolarized (*cross-centered triangle*) holding potentials. The degree of inhibition at the two holding potentials was obtained by normalizing inhibited currents by their corresponding control currents (hyperpolarized inhibition = ▲ ÷ △; depolarized inhibition = ● ÷ ○).

Results of this experiment for each of three classes of channels are reported in separate columns in Fig. 4, as labeled. At the top of each column (A–C) is a diary plot of peak current. Shown below is the degree of inhibition at hyperpolarized and depolarized holding potentials. For each channel type, inhibition was clearly greater at the depolarized holding potential, which is consistent with state-dependent block of all channels by verapamil.

Fig. 5 summarizes results for the same holding potential experiment with diltiazem, using the identical format. Here, only α_{1C} showed greater inhibition at the depolarized holding potential (Fig. 5A); α_{1A} and α_{1E} were inhibited to the same extent (Figs. 5, B and C), regardless of holding potential. These results support the view that only α_{1C} showed state-dependent block by diltiazem.

Unequivocal support for the results of these two-point holding potential experiments came with quantitative shape analysis of complete steady state inactivation (h_∞) curves, obtained in the presence and absence of drug. Following the same rationale as the streamlined holding potential protocol above, state-dependent blockade should not only depress the h_∞ curve but also shift its position after renormalization. State-independent block should depress the h_∞ curve without a shift in position. Fig. 6 shows the results of such an experiment, in which h_∞ curves were obtained with 20-sec prepulses to various voltages. Data for the three classes of channels are presented in separate columns, as labeled. At the top are shown h_∞ curves obtained in the absence (*open symbol*) and presence (*filled symbol*) of verapamil. In each case, there was a substantial depression *of* h_∞ curves by verapamil. At the bottom are shown two h_∞ curves after normalization to facilitate shape comparison. Clearly, there were changes in shape with drug inhibition of all channels, which is consistent with state-dependent inhibition throughout. Fig. 7 summarizes identical experiments, now with diltiazem as the blocker. After normalization of h_∞ curves (*bottom*, A–C), only α_{1C} gave evidence of state-dependent block.

Structural determinants of state-dependent block by benzothiazepines. Taken together, the r_{100} (Figs. 1 and 2), dose-response (Fig. 3), and holding-potential (Figs. 4–7) experiments provided good evidence that a benzothiazepine produced state-dependent block of only α_{1C} channels, not α_{1A} or α_{1E} channels. This clear distinction in a fundamental pharmacological property furnished us a novel opportunity to apply chimeric and mutant Ca^{2+} channel analysis to gain insight into the structural determinants of state-dependent block.

According to the guarded-receptor hypothesis of drug block, the drug-binding site and guard elements that control drug access to the binding site are physically distinct structures (18). Critical amino acids for diltiazem binding have been localized to IVS6 (12), with potential ancillary contri-

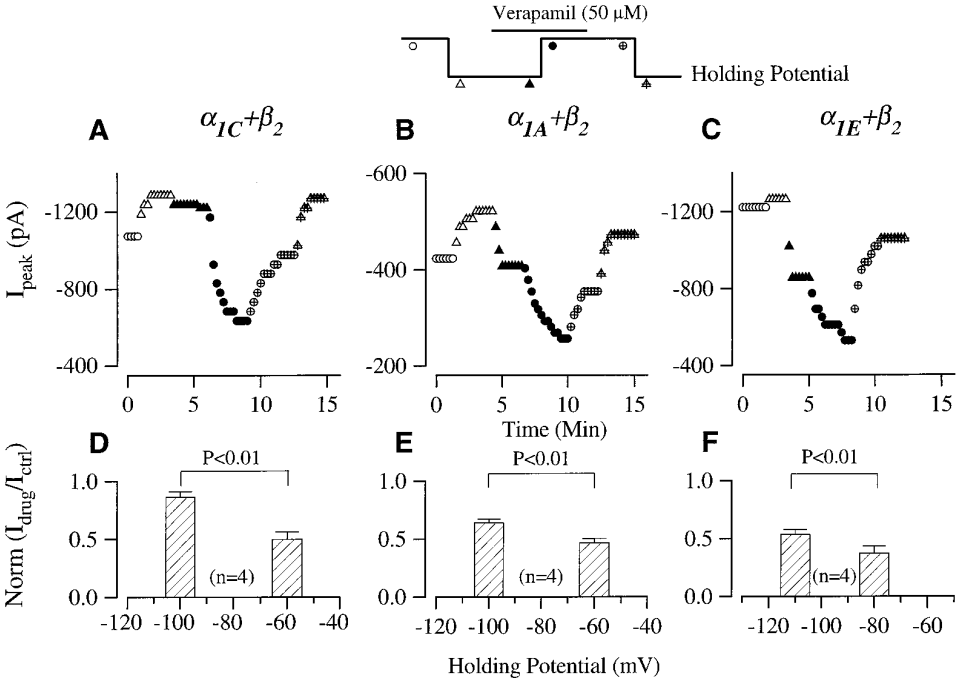

Fig. 4. Effect of holding potential on verapamil inhibition. *Top*, diagram of holding potentials used in the protocol described below. A–C, Diary plots of peak current measured during various phases of protocol. D–F, Extent of verapamil inhibition at different holding potentials for (D) α_{1C}, (E) α_{1A}, and (F) α_{1E}. *Ordinate*, fraction of control current remaining in the presence of verapamil. Statistical significance was from *n* cells as indicated. Brief test pulses to +10 mV were delivered every 15 sec from the indicated holding potentials, with 5 mM Ca^{2+} as charge carrier. Before the application of verapamil, we set the holding potential to a depolarized level, where the channel populated deep resting, shallow resting, and inactivated states. After stabilization at this potential (○), we changed the holding potential to a hyperpolarized value while still in the absence of verapamil. After equilibration (△), inactivation was minimized, and most channels populated deep resting states. The control currents obtained at these two potentials served to normalize currents inhibited by verapamil. While maintaining the hyperpolarized holding potential, verapamil was applied, and the steady state level of inhibition was allowed to develop (▲). The holding potential was then adjusted to the initial depolarized level, and the steady level of inhibition was allowed to develop with verapamil still present (●). Verapamil was then removed, and the current was allowed to recover at the depolarized (*cross-centered circle*) and hyperpolarized (*cross-centered triangle*) holding potentials. The degree of inhibition at the two holding potentials was obtained by normalizing inhibited currents by their corresponding control currents (hyperpolarized inhibition = ▲ ÷ △; depolarized inhibition = ● ÷ ○). We chose verapamil concentrations of (B) 30 μM for α_{1A}, (A) 50 μM for α_{1C}, and (C) 100 μM for α_{1E}, at which comparable degrees of inhibition were produced at holding potentials of −110 to −100 mV.

bution from IIIS6 (13). We therefore wondered whether structures specifying properties of state dependence were located on repeats III and IV near the binding site or could be entirely distinct structures residing on repeats I and II. Accordingly, we examined diltiazem blockade of chimeric Ca^{2+} channels in which repeats I and II were interchanged between α_{1C} and α_{1A}. The resulting chimeric channels are schematized in Fig. 8 (*top*). The profile of diltiazem blockade for the two constructs appear in separate columns, as labeled. Both channel constructs were readily inhibited by 200 μM diltiazem, as demonstrated in Fig. 8, A and B, by the exemplar current records (*top*) and the diary plots of peak current (*bottom*). Interestingly, the recovery from inhibition was rapid in α_{1CCAA} but slow in α_{1AACC}, suggesting that the characteristic slow recovery of α_{1C} (Fig. 2A) was mediated by structures in repeats III and IV near the binding site. The most important new findings came with the effects of diltiazem on the decay rate of currents. Close inspection of the exemplar traces shows that diltiazem hardly affected the waveform of α_{1CCAA} (Fig. 8A, *top*) but significantly accelerated the decay of current of α_{1AACC} (Fig. 8B, *top*). The r_{100} diaries, shown below in Fig. 8, C and D, confirm these impressions, which argue for the predominance of repeats III and IV in mediating the state-dependent phenotype.

Such predominance of repeats III and IV gave reason to wonder whether the very amino acids that are critical for higher affinity diltiazem binding in α_{1C} (12) are also essential to the state-dependent phenotype. A tyrosine, an alanine, and an isoleucine located in IVS6 of α_{1C} (Y1490, A1494, and I1497 in the rabbit cardiac α_{1C} used here) have been proposed to be crucial to diltiazem inhibition; when the corresponding amino acids in α_{1A} are mutated to these amino acids, higher affinity diltiazem blockade is conferred to the α_{1A} backbone (12). Here, we performed the converse experiment and mutated the critical amino acids in α_{1C} to their α_{1A} counterparts. We then asked whether these amino acids alone, which are a critical part of the binding pocket, are essential to the state-dependent phenotype.

Fig. 9 shows the effects of diltiazem on the resulting construct, $\alpha_{1C\text{-}ISM}$. The exemplar currents and diary plot (Fig. 9A) demonstrate the ready block of peak current by diltiazem, although the half-maximal inhibitory concentration was increased by ~10-fold (not shown). More telling was the effect of diltiazem on the decay of current in the exemplar records. In addition to the substantial inhibition of current, diltiazem still produced a marked acceleration of the current decay. This impression was confirmed by the obvious decline in the diary plot of r_{100} during diltiazem application (Fig. 9B, *bottom*). These results suggested that diltiazem still prefer-

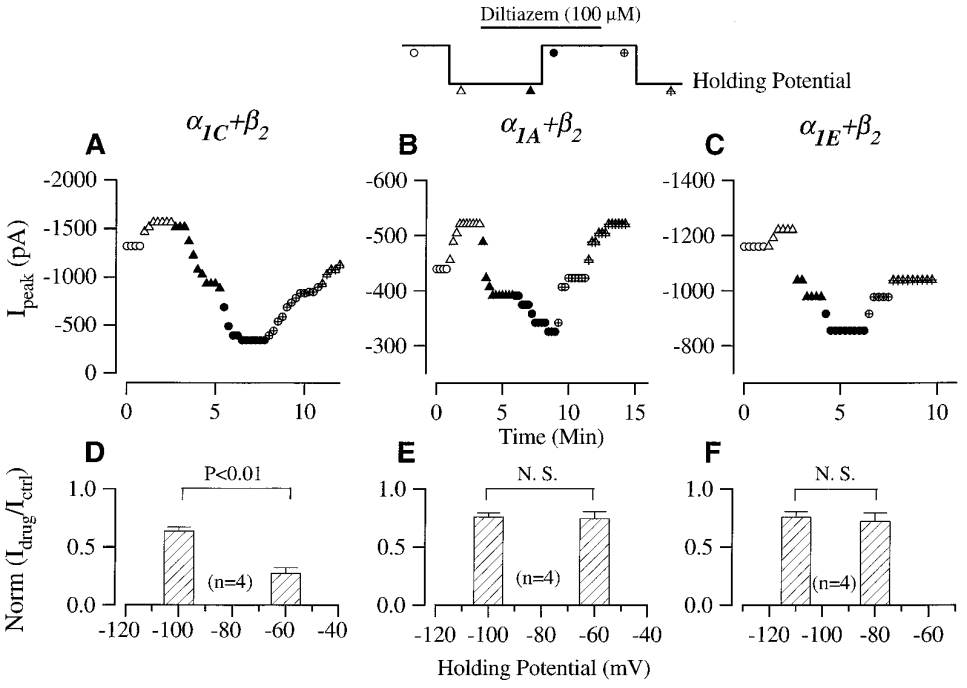

Fig. 5. Effect of holding potential on diltiazem inhibition. The format and protocol are identical to those in Fig. 4, except that 100 μM diltiazem was used for drug inhibition throughout.

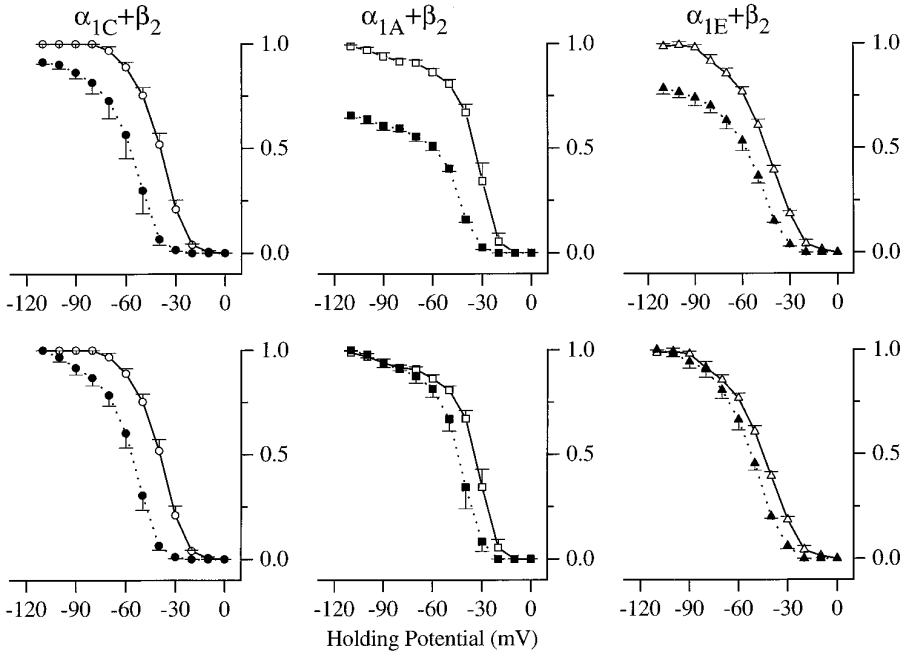

Fig. 6. Effect of verapamil on steady state inactivation (h_∞) curves. Data for three classes of channels are presented in separate columns as labeled. *Top*, h_∞ curves obtained in the (*open*) absence and (*filled*) presence of 50 μM verapamil. *Ordinate*, peak test currents after normalization by the peak test current obtained following a prepulse to −110 mV in the absence of drug. *Bottom*, two h_∞ curves, after normalization to facilitate shape comparison. All channel types show shifts along the voltage axis. Protocol, every 60 sec, test depolarizations to +10 mV were delivered after a 20-sec prepulse to voltages from −110 mV to 0 mV. The holding potential was −110 mV throughout. The charge carrier was 5 mM Ca^{2+}. Separate groups of cells were averaged for (*open*) control and (*filled*) drug data. Each group contained four or five cells.

entially inhibited channels in the open and/or inactivated states.

To bolster the idea that diltiazem block of $\alpha_{1C\text{-}ISM}$ was state dependent, we examined the holding-potential dependence of diltiazem blockade of $\alpha_{1C\text{-}ISM}$. Fig. 9, C and D, summarizes the results of a two-point holding potential experiment that is identical in every regard to that reported for α_{1C} in Fig. 5, A and D. The data clearly argue that there was still an appreciable effect of holding potential on diltiazem blockade.

The experiments shown in Fig. 9 consistently demonstrate that there must be other distinct structural elements in repeats III and IV, different from the amino acids most critical to diltiazem binding (Y1490, A1494, I1497), that are essential for state-dependent blockade. This result has important structural implications on which we elaborate in the Discussion.

Discussion

We report on the first systematic characterization of phenylalkylamine and benzothiazepine inhibition of three molecular classes of Ca^{2+} channels (α_{1A}, α_{1E}, and α_{1C}), expressed individually from recombinant clones. Although phenylalkylamines and benzothiazepines were developed as blockers of L-type (α_{1C}) channels, we find that verapamil and diltiazem inhibit all three classes of channels tested, with

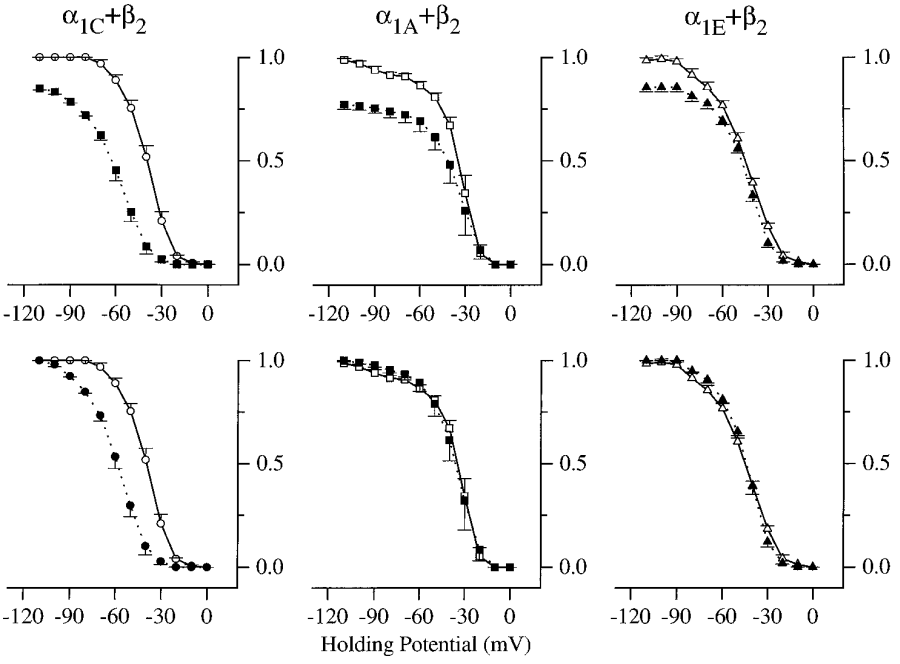

Fig. 7. Effect of diltiazem inhibition on steady state inactivation (h_∞) curves. Data for the three classes of channels are presented in separate columns as labeled. The format is identical to that in Fig. 6, except that 100 μM diltiazem was used for drug inhibition. After normalization to facilitate shape comparison (*bottom row*), shifts along the voltage axis are apparent for only α_{1C}; the normalized h_∞ relations for α_{1A} and α_{1E} essentially superimpose, arguing for state-independent block. Control and drug data were averaged from different groups of cells. The control (*open*) data are replotted from Fig. 6. The drug (*filled*) data are averaged from four or five cells in each group.

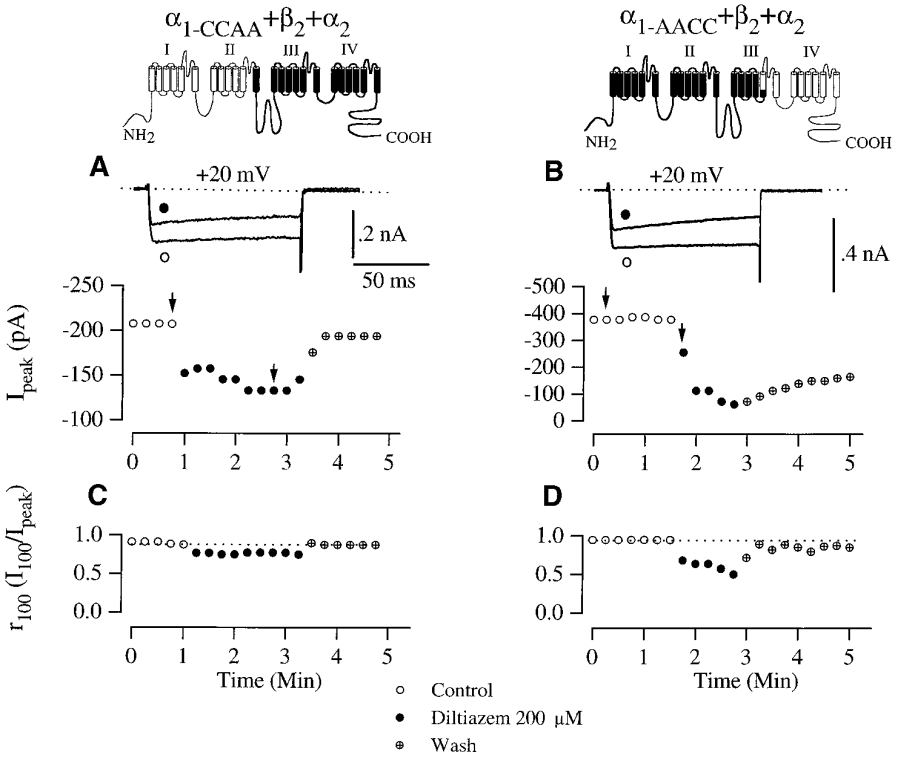

Fig. 8. Diltiazem inhibition of chimeric Ca^{2+} channels, derived from α_{1C} and α_{1A}. *Left*, data for $\alpha_{1\text{-CCAA}}$. *Top left*, chimera diagrammed (*dark portions* are derived from α_{1A}). *Right*, results for $\alpha_{1\text{-AACC}}$. *Top right*, diagram. A and B (*top*), exemplar current traces (○) before and (●) during exposure to 200 μM diltiazem. A and B (*bottom*), diary plots of peak current (○) before, (●) during, and (*cross-centered circle*) after exposure to 200 μM diltiazem. *Arrows*, traces shown above. C and D, diary plots of r_{100}, the fraction of peak current remaining at the end of 100-msec depolarization. These demonstrate that diltiazem produced little change in current decay of (C) $\alpha_{1\text{-CCAA}}$, in contrast to obvious acceleration of current decay of (D) $\alpha_{1\text{-AACC}}$. C, For $\alpha_{1\text{-CCAA}}$, the average change in r_{100} (drug − control) was small (−0.07 ± 0.04; three cells) and lacked statistical significance. D, In contrast, for $\alpha_{1\text{-AACC}}$, the change in r_{100} was large (−0.26 ± 0.06; four cells) and significant ($p < 0.05$). Test depolarizations were delivered every 15 sec from a holding potential of −80 mV, with 30 mM Ba^{2+} as charge carrier. Both chimeric α_1 constructs were coexpressed with β_2 and α_2 subunits.

half-maximal inhibitory concentrations that differ by less than several-fold (Fig. 3). There are striking qualitative differences in the state dependence of inhibition observed in different drug/channel combinations. Although verapamil shows evidence of state-dependent inhibition in all three channels, diltiazem produces state-dependent block of only α_{1C} channels (not α_{1A} and α_{1E} channels). The determination of state dependence is based on mutually consistent results from current decay (Figs. 1 and 2), dose-response (Fig. 3), and holding-potential (Figs. 4–7) experiments. This is the first instance in which an organic Ca^{2+} channel blocker demonstrates similar overall potency in different channels but a fundamental difference in the state-dependent character of blockade. Verapamil, D888, and mibefradil all show signs of state-dependent blockade of several molecular classes of Ca^{2+} channels (9–11, 35).

Relation to previous studies. For channel/drug combinations that manifest state-dependent blockade, the extent of blockade will vary considerably depending on the holding potential (Figs. 6 and 7) and stimulation rate. Therefore, in comparing the half-maximal inhibitory concentrations specified in Fig. 3 with those in the literature (12), it is worth

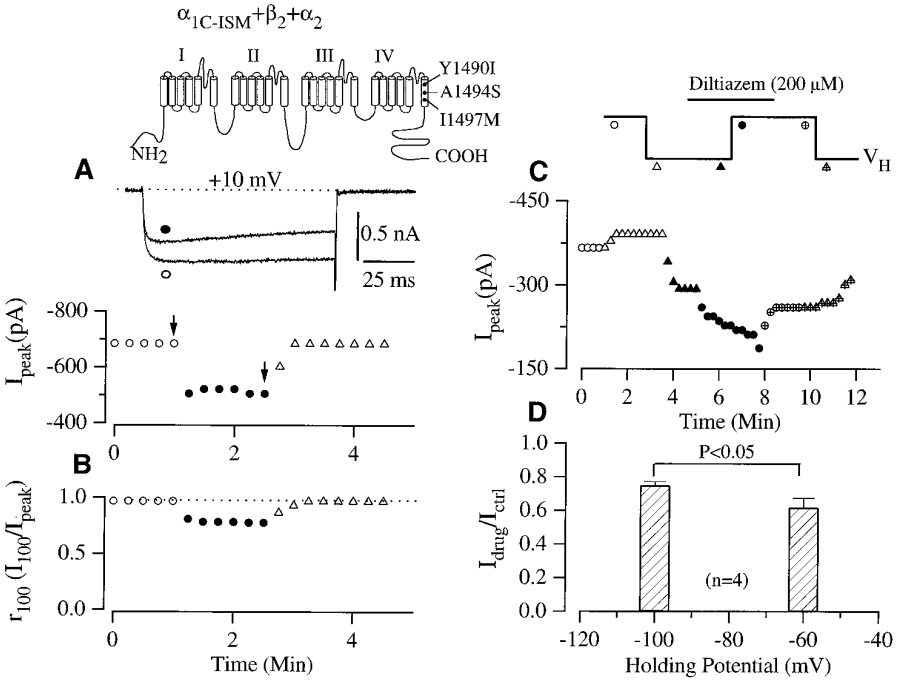

Fig. 9. Diltiazem inhibition of $\alpha_{1C\text{-}ISM}$, an α_{1C} construct in which three point mutations in IVS6 have been made to remove the high affinity coordinating sites for diltiazem (Y1490I, A1494S, I1497M). *Top*, location of the point mutations is diagrammed. A (*top*), exemplar current traces (○) before and (●) during exposure to 200 μM diltiazem. A (*bottom*), diary plots of peak current (○) before, (●) during, and (▲) after exposure to 200 μM diltiazem. *Arrows*, traces shown above. B, Diary plot of r_{100}, the fraction of peak current remaining at the end of 100-msec depolarization, corresponding to the same cell and protocol as in A. The depression of r_{100} with diltiazem demonstrates obvious speeding of current decay with drug application. For the exemplar experiment (A and B), 5 mM Ba^{2+} was the charge carrier. There was no difference in the change of r_{100} upon drug application with Ba^{2+} or Ca^{2+} serving as charge carrier. Overall, the change in r_{100} was large and reproducible, averaging -0.16 ± 0.02 ($p < 0.01$ for seven cells: three with 5 mM Ba^{2+} and four with 5 mM Ca^{2+} as charge carrier). C, Diary plot of peak current measured during various phases of holding potential (V_H) protocol diagrammed (*top*). Protocol was identical to that in Fig. 5. D, Extent of diltiazem inhibition at different holding potentials, derived from diary plots as in C. Statistical significance was assessed from four cells, with 5 mM Ca^{2+} as charge carrier. $\alpha_{1C\text{-}ISM}$ was coexpressed with β_2 and α_2 subunits throughout.

emphasizing that the data in these figures were obtained with a uniform holding potential and stimulation rate (−80 mV and 1/15 Hz, respectively). In instances in which there was considerable state-dependent blockade, the half-blocking concentration would certainly have been lower with depolarization of the holding potential and/or increase in the stimulation rate.

Our finding of selective state dependence of diltiazem blockade with α_{1C} (but not with α_{1A} and α_{1E}) contrasts somewhat with another study (12) in which recombinant α_{1A} currents, expressed in *Xenopus laevis* oocytes, showed evidence of state-dependent diltiazem blockade. The difference may arise from the use of different α_{1A} clones [rat brain in our case (24) versus rabbit brain in the other study (36)] or different β subunits [rat brain β_2 in our case (20) versus rabbit skeletal β_{1a} (37)]. In the former case, it may be that a restricted number of differences between the two α_{1A} clones account for the difference in state dependence, but it is interesting that our finding of state-independent diltiazem block extends to a construct as different as α_{1E}. Differences in pharmacological profile related to alternative splicing (38) looms as another possibility with enormous therapeutic potential. Further work is clearly necessary to characterize the structural determinants of the state-dependent phenotype.

Implications for drug discovery. The finding that diltiazem blocks only α_{1C} in a state-dependent manner gives reason to expect that there exist organic compounds that would demonstrate selective state-dependent blockade of certain neuronal Ca^{2+} channels. Our results with diltiazem argue that the general functional requirements of Ca^{2+} channels have not imposed common structural themes that require organic compounds to demonstrate similar state-dependent blocking properties across channels, as in the case of verapamil. In fact, eliprodil, an organic drug initially developed as an *N*-methyl-D-aspartate channel antagonist, seems to demonstrate selective blockade of N-type (α_{1B}) and P/Q-type (α_{1A}) channels while sparing L-type (α_{1C}) and R-type (α_{1E}) channels (39). There is great interest in discovering organic compounds with selectivity for neuronal channels because they may prove to be easier to obtain and deliver than neuropeptides, which despite their proven selectivity for particular types of neuronal channels, may have difficulty crossing the blood-brain barrier to reach targets in the central nervous system (35).

Molecular basis of state-dependent diltiazem blockade. Chimeric Ca^{2+} channel analysis between α_{1C} and α_{1A} localized most of the structural determinants for state-dependent diltiazem blockade to repeats III and IV of α_{1C}, which likely contain the elements required for benzothiazepine binding (12, 13). Analysis of $\alpha_{1C\text{-}ISM}$, a construct in which the predominant structural determinants of higher-affinity diltiazem inhibition of α_{1C} have been changed to their α_{1A} counterparts, revealed that state-dependent diltiazem inhibition was spared, despite a ~10-fold increase in half-maximal inhibitory concentration relative to α_{1C}. These results suggest that although the elements responsible for

state dependence ("guards") are largely contained within repeats III and IV, they may be structurally distinct from the most critical part of the actual binding region in IVS6. The existence of physically distinct elements controlling drug binding and access to the receptor fits naturally with a guarded-receptor (18) rather than a modulated receptor mechanism of drug inhibition (16, 17). Such a physical dissociation of elements controlling binding and access has also been demonstrated in voltage-gated Na^+ channels (40). It will be interesting to see whether such a physical distinction turns out to be a general design theme for state-dependent block of all voltage-gated channels.

Acknowledgments

We are grateful to Dr. Shao-kui Wei (Johns Hopkins University School of Medicine) for his collaboration on certain experiments, to Yan Wang for constructing $\alpha_{1CSfuI+}$, and to Dr. Paul Fuchs, David Brody, Lisa Jones, and Parag Patil for discussion and comments. We acknowledge the following individuals for generously providing Ca^{2+} channel clones: Terry P. Snutch (University of British Columbia, Vancouver, British Columbia, Canada) (α_{1A}, α_{1E}, α_2), Edward Perez-Reyes (Loyola University, Chicago, IL) (α_{1C}, β_{2a}), and the late Chris Wei (Georgia Medical College) (α_{1C}).

References

1. Olivera, B. M., G. P. Miljanich, J. Ramachandran, and M. E. Adams. Calcium channel diversity and neurotransmitter release: the *omega*-conotoxins and *omega*-agatoxins. *Annu. Rev. Biochem* **63:**823–867 (1994).
2. Fleckenstein, A. History of calcium antagonist. *Circ Res.* **52:**I3–I16 (1983).
3. Janis, R. A., and D. J. Triggle. Drugs action on calcium channels, in *Calcium Channels: Their Properties, Functions, Regulation, and Clinic Relevance* (L. D. Partridge and J. K. Leach, eds.). CRC Press, Boca Raton, FL, 195–249 (1991).
4. McDonald, T. F., S. Pelzer, W. Trautwein, and D. J. Pelzer. Regulation and modulation of calcium channels in cardiac, skeletal, and smooth muscle cells. *Physiol. Rev.* **74:**365–507 (1994).
5. Xiao, W. H., and G. J. Bennett. Synthetic ω-conopeptides applied to the site of nerve injury suppress neuropathic pains in rats. *J. Pharmacol. Exp. Ther.* **274:**666–672 (1995).
6. Ophoff, R. A., G. M. Terwindt, M. N. Vergouwe, R. van Eijk, P. J. Oefner, S. M. G. Hoffman, J. E. Lmerdin, H. W. Mohrenweiser, D. E. Bulman, M. Ferrari, J. Haan, D. Lindhout, G.-J. B. van Ommen, M. H. Hofker, M. D. Ferrari, and R. R. Frants. Familial hemiplegic migraine and episodic ataxia type-2 are caused by mutations in the Ca^{2+} channel gene CACNL1A4. *Cell* **87:**543–552 (1996).
7. Grabner, M., Z. Wang, S. Hering, J. Striessnig, and H. Glossmann. Transfer of 1,4-dihydropyridine sensitivity from L-type to class A (BI) calcium channels. *Neuron* **16:**207–218 (1996).
8. Peterson, B. Z., T. N. Tanada, and W. A. Catterall. Molecular determinants of high affinity dihydropyridine binding in L-type calcium channels. *J. Biol. Chem.* **271:**5293–5296 (1996).
9. Schuster, A., L. Lacinova, N. Klugbauer, H. Ito, L. Birnbaumer, and F. Hofmann. The IVS6 segment of the L-type calcium channel is critical for the action of dihydropyridines and phenylalkylamines. *EMBO J.* **15:**2365–2370 (1996).
10. Hockerman, G. H., B. D. Johnson, T. Scheuer, and W. A. Catterall. Molecular determinants of high affinity phenylalkylamine block of L-type calcium channels. *J. Biol. Chem.* **270:**22119–22122 (1995).
11. Doring, F., V. E. Degtiar, M. Grabner, J. Striessnig, S. Hering, and H. Glossmann. Transfer of L-type calcium channel IVS6 segment increases phenylalkylamine sensitivity of α_{1A}. *J. Biol. Chem.* **271:**11745–11749 (1996).
12. Hering, S., S. Aczel, M. Grabner, F. Doring, S. Berjukow, J. Mitterdorfer, M. J. Sinnegger, J. Striessnig, V. E. Degtiar, Z. Wang, and H. Glossmann. Transfer of high sensitivity for benzothiazepine from L-type to class A calcium channels. *J. Biol. Chem.* **271:**24471–24475 (1996).
13. Kraus, R., B. Reichl, S. D. Kimball, M. Grabner, B. J. Murphy, W. A. Catterall, and J. Striessnig. Identification of benz(othi)azepine binding regions within L-type calcium channel α_1 subunits. *J. Biol. Chem.* **271:**20113–20118 (1996).
14. Diochot, S., S. Richard, M. Baldy-Moulinier, J. Nargeot, and J. Valmier. Dihydropyridines, phenylalkylamines and benzothiazepines block N-, P/Q- and R-type calcium currents. *Pflueg. Arch. Eur. J. Physiol.* **431:**10–19 (1995).
15. Ishibashi, H., A. Yatani, and N. Akaike. Block of P-type Ca^{2+} channels in freshly dissociated rat cerebellar Purkinje neurons by diltiazem and verapamil. *Brain Res.* **695:**88–91 (1995).
16. Hille, B. Local anesthetics: hydrophilic and hydrophobic pathways for the drug-receptor reaction. *J. Gen. Physiol.* **69:**497–515 (1977).
17. Hondeghem, L. M., and B. G. Katzung. Time- and voltage-dependent interactions of antiarrhythmic drugs with cardiac sodium channels. *Biochim. Biophys. Acta* **472:**373–398 (1977).
18. Starmer, C. F., A. O. Grant, and H. C. Strauss. Mechanisms of use-dependent block of sodium channels in excitable membranes by local anesthetics. *Biophys. J.* **46:**15–27 (1984).
19. Randall, A., and R. W. Tsien. Pharmacological dissection of multiple types of Ca^{2+} channel currents in rat cerebellar granule neurons. *J. Neurosci.* **15:**2995–3012 (1995).
20. Perez-Reyes, E., A. Castellano, H. S. Kim, P. Bertrand, E. Baggstrom, A. E. Lacerda, X. Y. Wei, and L. Birnbaumer. Cloning and expression of a cardiac/brain β subunit of the L-type calcium channel. *J. Biol. Chem.* **267:**1792–1797 (1992).
21. Tomlinson, W. J., A. Stea, E. Bourinet, P. Charnet, J. Nargeot, and T. P. Snutch. Functional properties of a neuronal class C L-type calcium channel. *Neuropharmacology* **32:**1117–1126 (1993).
22. Wei, X. Y., E. Perez-Reyes, A. E. Lacerda, G. Schuster, A. M. Brown, and L. Birnbaumer. Heterologous regulation of the cardiac Ca^{2+} channel α_1 subunit by skeletal muscle β and γ subunits: implications for the structure of cardiac L-type Ca^{2+} channels. *J. Biol. Chem.* **266:**21943–7 (1991).
23. Soong, T. W., A. Stea, C. D. Hodson, S. J. Dubel, S. R. Vincent, and T. P. Snutch. Structure and functional expression of a member of the low voltage-activated calcium channel family. *Science (Washington D. C.)* **260:**1133–1136 (1993).
24. Starr, T. V., W. Prystay, and T. P. Snutch. Primary structure of a calcium channel that is highly expressed in the rat cerebellum. *Proc. Natl. Acad. Sci. USA* **88:**5621–5625 (1991).
25. Stea, A., W. J. Tomlinson, T. W. Soong, E. Bourinet, S. J. Dubel, S. R. Vincent, and T. P. Snutch. Localization and functional properties of a rat brain α_{1A} calcium channel reflect similarities to neuronal Q- and P-type channels. *Proc. Natl. Acad. Sci. USA* **91:**10576–10580 (1994).
26. Gorman, C. M., D. R. Gies, and G. McCray. Transient production of proteins using an adenovirus transformed cell line. *DNA Prot. Eng. Techniques* **2:**3–10 (1990).
27. Dhallan, R. S., K. W. Yau, K. A. Schrader, and R. R. Reed. Primary structure and functional expression of a cyclic nucleotide-activated channel from olfactory neurons. *Nature (Lond.)* **347:**184–187 (1990).
28. Kaufman, R. J. Identification of the components necessary for adenovirus translational control and their utilization in cDNA expression vectors. *Proc. Natl. Acad. Sci. USA* **82:**689–693 (1985).
29. Wei, X., A. Neely, A. E. Lacerda, R. Olcese, E. Stefani, E. Perez-Reyes, and L. Birnbaumer. Modification of Ca^{2+} channel activity by deletions at the carboxyl terminus of the cardiac α_1 subunit. *J. Biol. Chem.* **269:**1635–1640 (1994).
30. Higuchi, R. Using PCR to engineer DNA, in *PCR Technology* (H. A. Erlich, ed.). Stockton Press, Basingstoke, Hants, UK, 61–70 (1989).
31. Lee, K. S., and R. W. Tsien. Mechanism of calcium channel blockade by verapamil, D600, diltiazem and nitrendipine in single dialysed heart cells. *Nature (Lond.)* **302:**790–794 (1983).
32. Bean, B. P. Nitrendipine block of cardiac calcium channels: high-affinity binding to the inactivated state. *Proc. Natl. Acad. Sci. USA* **81:**6388–6392 (1984).
33. Kass, R. S., and D. S. Krafte. Negative surface charge density near heart calcium channels: relevance to block calcium channels. *J. Gen. Physiol.* **89:**629–644 (1987).
34. McDonald, T. F., D. Pelzer, and W. Trautwein. Cat ventricular muscle treated with D600: effects on calcium and potassium currents. *J. Physiol. (Lond)* **352:**203–216 (1984).
35. Bezprozvanny, I., and R. W. Tsien. Voltage-dependent blockade of diverse types of voltage-gated Ca^{2+} channels expressed in *Xenopus* oocytes by the Ca^{2+} channel antagonist mibefradil (Ro 40–5967). *Mol. Pharmacol.* **48:**540–549 (1995).
36. Mori, Y., T. Friedrich, M.-S. Kim, A. Mikami, K. Nakai, P. Ruth, E. Rosse, F. Hoffmann, V. Flockerzi, T. Furuichi, K. Mikoshiba, K. Imoto, T. Tanabe, and S. Numa. Primary structure and functional expression from complementary DNA of brain calcium channel. *Nature (Lond.)* **350:**398–402 (1991)
37. Ruth, P., A. Rohrkasten, M. Miel, E. Bosse, S. Regulla, H. E. Meyer, V. Flockerzi, and F. Hoffmann. Primary structure of the β subunit of the DHP-sensitive calcium channel from skeletal muscle. *Science (Washington D.C.)* **245:**1115–1118 (1989).
38. Sakurai, T., R. E. Westenbroek, J. Rettig, J. Hell, and W. A. Catterall. Biochemical properties and subcellular distribution of the BI and rBA isoforms of α_{1A} subunits of brain calcium channels. *J. Cell Biol.* **134:**511–528 (1996).
39. Avenet, P., B. Biton, H. Depoortere, and B. Scatton. Neuroprotective compound eliprodil (SL 82.0715) blocks N-, P- but not L-type Ca^{2+} channels in rat cultured cerebellar granule cells. *Soc. Neurosci. Abstr.* **22:**689.5 (1996).
40. Ragsdale, D., J. C. McPhee, T. Scheuer, and W. A. Catterall. Molecular determinants of state-dependent block of Na^+ channels by local anesthetics. *Science (Washington D. C.)* **265:**1724–1728 (1994).

Send reprint requests to: David T. Yue, M.D., Ph.D., Program in Molecular and Cellular System Physiology, Department of Biomedical Engineering, Johns Hopkins University School of Medicine, 720 Rutland Avenue, Baltimore, MD 21205. E-mail: dyue@bme.jhu.edu